THE PENNSYLVANIA STATE UNIVERSITY
SCHREYER HONORS COLLEGE

DEPARTMENT OF CHEMICAL ENGINEERING

PLASMID TRANSMISSION THROUGH NUCLEPORE TRACK ETCHED MEMBRANES

ALLISON BETH HARTER
Spring 2010

A thesis
submitted in partial fulfillment
of the requirements
for baccalaureate degrees
in Chemical Engineering and French
with honors in Chemical Engineering

Reviewed and approved* by the following:

Andrew Zydney
Department Head of Chemical Engineering
Thesis Supervisor

Ali Borhan
Professor of Chemical Engineering
Honors Adviser

* Signatures are on file in the Schreyer Honors College.

Abstract

Recent results have demonstrated that ultrafiltration can be effectively used for the large-scale purification of plasmid DNA for the production of gene therapy agents and DNA-based vaccines. The objectives of this thesis were to obtain experimental data for: (1) plasmid transmission through a series of track-etched (Nuclepore) membranes with very uniform pores to examine the role of the pore size distribution, and (2) the effect of membrane porosity on plasmid ultrafiltration. Experiments were performed with Nuclepore track-etched membranes with pore sizes of 15, 30, and 50 nm using a linearized 3 kilobase pair plasmid at both low and high salt concentrations. A low porosity version of the 50 nm pore size membrane was produced by blocking a percentage of the pores with polystyrene microspheres that were subsequently held in place by melting the polystyrene. Plasmid transmission was negligible below a critical value of the filtrate flux but then increased to nearly 100% transmission at high filtrate flux. The increase in plasmid transmission occurred over an approximately 9-fold range in filtrate flux, which is very similar to the transition seen previously with composite regenerated cellulose membranes that have a broad pore size distribution. These results strongly suggest that the gradual transition in sieving is unrelated to the breadth of the pore size distribution. The critical flux for plasmid transmission for the low porosity membrane was significantly smaller than that for the unmodified Nuclepore membrane, with the observed dependence on membrane porosity in good agreement with theoretical predictions of an elongational flow model previously developed to describe transmission of a flexible polymer through a cylindrical pore. These data provide the first direct verification of the predicted dependence on membrane porosity, while

also giving additional insights into the physical phenomena controlling plasmid transmission through small pore size ultrafiltration membranes.

Table of Contents

Acknowledgements

I would like to thank everyone who helped me complete this thesis. Persevering through all of the research was, at times, one of the most difficult things I have done during my undergraduate career at Penn State, and I would not have been successful without all of the support I received.

I would like to thank Dr. Zydney for all of his advice and support throughout the research and writing of my thesis. I really appreciate being able to work in his lab over the past 5 years.

I would also like to thank David Latulippe for always taking the time to teach me the skills and concepts I needed in the lab. In addition to the techniques related specifically to this research, Dave has also taught me the importance of creating an experiment to collect meaningful data.

I appreciate all of the help that everyone in Dr. Zydney and Dr. Cirino's labs have given me throughout my time doing research.

Finally, I would like to thank my family and friends for always believing that I could do a great job, even when I was struggling, and for listening to me talk about my thesis incessantly for the past few months.

1. Introduction

Plasmids are closed, double stranded pieces of DNA which carry genetic information outside of the chromosome. Plasmid DNA is of current interest for both gene therapy and DNA-based vaccines. In gene therapy applications, a plasmid containing a specific gene coding for a protein of interest is administered to the patient. Clinical trials are currently underway for the treatment of cystic fibrosis and muscular dystrophy, genetic disorders in which a critical chromosomal gene is absent or codes for a dysfunctional protein [1]. DNA vaccines are designed to elicit a strong immunological response by coding for a particular antigen, e.g. a protein from the capsid of the influenza virus. As of 2003, more than 600 different plasmids had been examined in clinical trials [2]. These plasmids are typically produced in *Escherichia coli* (*E. coli*) bacteria and are 5-10 kilobase pairs (kbp) in length. The supercoiled isoform of the plasmid is preferred for gene therapy applications since this form has the greatest transfection efficiency [3]. The linear isoform, formed when there is a break in both strands of the supercoiled DNA, is considered an impurity that needs to be removed during manufacturing.

Although laboratory-scale methods for purifying plasmid DNA are well-established, most of these techniques are impractical for industrial scale separations due to their high cost, low yield, and very low capacity. Effective doses for plasmid DNA therapeutics are still being established based on results from ongoing clinical trials, but current estimates are on the order of milligrams, which will require the production and purification of up to 50 g of DNA per batch [2]. This level of production will require the development of new and more efficient processes that can achieve the high degree of plasmid DNA purification required for therapeutic use.

Membrane microfiltration and ultrafiltration can both be used for plasmid production and purification. Microfiltration can be used to concentrate and wash the *E. coli*, thereby removing extracellular impurities prior to cell lysis. Microfiltration through 0.2 μm pore size membranes can also be used for sterile filtration of final products. Ultrafiltration has been examined for removal of small RNA and protein impurities, and it can also be used for concentration and final formulation of the therapeutic plasmid [3]. However, the bulk of the plasmid purification is typically accomplished by size exclusion and ion exchange chromatography. Most chromatographic media have very low capacity for plasmid purification, in part because the pore size of the porous particles was originally optimized for the purification of small proteins [2]. The net result is that chromatography provides a significant fraction of the total process costs for DNA purification [1]. There is thus significant interest in the development of new, lower cost, technologies for DNA purification, including the possibility of using membrane systems to remove a wide range of impurities such as undesired DNA isoforms [4].

Kong et al. studied the effect of filtrate flux and DNA feed concentration on DNA transmission through 0.22 μm polyvinylidene fluoride (PVDF) membranes [5]. Transmission was found to be independent of both filtrate flux and initial DNA concentration. However, DNA transmission did decrease with increasing DNA size for plasmids from 6 kbp to 116 kbp. Adsorption of DNA to the membrane was found to be negligible, although there was evidence of DNA degradation for the larger plasmids at high filtrate flux. Plasmid transmission also increased in the presence of 150 mM sodium chloride (NaCl), suggesting a role for either intra- or inter-molecular electrostatic interactions.

Latulippe et al. obtained very extensive data for the transmission of a 3 kpb plasmid through composite regenerated cellulose membranes as a function of the filtrate flux [6]. The

sieving coefficient was essentially zero at low values of the filtrate flux, but increased rapidly at higher filtrate flux. This behavior was not due to concentration polarization effects, i.e. the accumulation of retained plasmid at the upstream surface of the membrane, as the stirring speed (bulk mass transfer rate) had no effect on plasmid transmission. Instead, the increase in plasmid transmission with increasing filtrate flux was due to the elongation of the plasmid in the converging flow field into the membrane pores. The data suggested that there was a critical value of the filtrate flux (J_{crit}) above which the plasmid sieving coefficient became significant. Experimental measurements of the critical flux for different pore size membranes were consistent with predictions of a modified elongational flow model:

$$J_{crit} = \left(\frac{\pi^2 D}{R_G^2}\right)\left(\frac{\varepsilon R_S^3}{r_p^2}\right) \qquad (1)$$

where D is the translational diffusion coefficient, r_p is the pore radius, ε is the membrane porosity, R_G is radius of gyration, and R_S is the radius of the plasmid superhelix.

Latulippe and Zydney performed a detailed study of the effects of salt concentration and type on plasmid transmission through ultrafiltration membranes [7]. The critical flux decreased with increasing NaCl concentration. At a given value of the filtrate flux, the sieving coefficient increased as much as 80-fold as the NaCl concentration increased from 1 to 150 mM. Latulippe and Zydney hypothesized that the increase in transmission was due to the reduction in effective size of the plasmid arising from the decrease in intramolecular electrostatic interactions at higher salt concentrations. Even greater effects were seen with divalent magnesium ions, with the addition of magnesium chloride ($MgCl_2$) causing a dramatic increase in plasmid transmission at a much lower salt concentration than that obtained with NaCl.

Although the modified elongational flow model (Equation 1) was in good qualitative agreement with the experimental data for the critical filtrate flux, this model predicts a very sharp

increase in transmission from near zero to essentially 100% when the flux becomes larger than J_{crit}. In contrast, experimental measurements of the plasmid sieving coefficient showed a fairly gradual increase in transmission with increasing flux, with the transmission increasing from zero to more than 50% as the flux varies by more than a factor of four. Latulippe and Zydney hypothesized that this gradual increase in transmission may have been due to the presence of a broad pore size distribution in the composite regenerated cellulose membranes used in their studies, but there was no independent validation of this assumption. In addition, there is currently no experimental data examining the effect of the membrane porosity (ε) on the value of the critical flux.

The objectives of the work performed in this thesis were to obtain experimental data for: (1) plasmid transmission through track-etched (Nuclepore) membranes with very uniform pores to examine the role of the pore size distribution on plasmid ultrafiltration, and (2) the effect of membrane porosity on plasmid transmission and the magnitude of the critical filtrate flux. The track-etched membranes used in this work were created by irradiating a thin polymeric film with fission fragments from heavy nuclei of a fissionable isotope (typically californium) or by using ion beams from accelerators [8], with the pores then formed by chemically etching the damage tracks in the polymer (typically using aqueous alkali solutions). Track-etched membranes have been used previously in small-scale separations [9], to verify predictions of hydrodynamic models for protein transport [10], and to study membrane fouling phenomena [11], but there are currently no experimental studies of plasmid filtration through these highly uniform pore size membranes.

2. Materials and Methods

2.1. Solution Preparation

Buffer solutions were prepared by diluting concentrated 100x Tris-EDTA (TE) buffer (Fluka) with deionized distilled (DI) water obtained from a NANOpure Diamond water purification system (Barnstead Thermolyne Corporation). Sodium chloride (NaCl, VWR) was added to achieve the desired ionic strength. All buffer solutions were filtered through 0.2 µm pore size filters to remove any particulates prior to use. The solution pH was measured using a 420APlus pH meter (Thermo Orion) and the conductivity was measured using a 105APlus Conductivity meter (Thermo Orion).

2.2. Linear Plasmid Preparation

A 3.0 kpb pBluescript® plasmid was obtained from Aldevron as the supercoiled isoform. The plasmid was linearized (cut in two locations) using the restriction enzyme BamHI (Invitrogen) dissolved in concentrated 10x REACT 3 buffer (Invitrogen). The plasmid, enzyme, and buffer solution were mixed and incubated for 3 hours at 37°C to allow for complete digestion. The resulting linear plasmid was purified by chromatography using a small centrifugal DNA Clean and Concentrator kit (Zymo Research). All plasmid samples were stored at -20°C until used in the ultrafiltration experiments.

The plasmids were thawed at 4°C immediately prior to use. The plasmids were then added to the appropriate buffer to obtain a solution with 250 ng/mL concentration of the linear

plasmid. The linear structure of the plasmid was verified using agarose gel electrophoresis using the procedures described later in this section.

2.3. Membrane Preparation

Nuclepore polycarbonate track-etched membranes (Whatman) were used for all ultrafltration experiments. Membranes with pore sizes of 15 nm (Lot #8060018), 30 nm (Lot #1140130), and 50 nm (Lot #1131013) were used. The membranes are made hydrophilic by addition of polyvinylpyrrolidone.

To create membranes with different porosities (pore densities), a fraction of the pores in the standard 50 nm pore size Nuclepore membrane were "blocked" using a procedure developed in our lab. A membrane was first placed in a 10 mL capacity ultrafiltration cell (Model 8010, Amicon Corp.) on top of a Tyvek support. The membrane was flushed with 20 mL of DI water using an applied pressure of 3 psi. The membrane hydraulic permeability was then evaluated using the procedure described in section 2.5. The stirred cell was moved to an oven (VWR, 1350FD) and used to filter 10 mL of a suspension of 67 nm carboxylate modified latex (polystyrene) microspheres (Invitrogen, Lot #448940) at room temperature using a pressure of 1.5 psi. The suspension was prepared by diluting the stock solution of microspheres ($2.5x10^{14}$ particles per mL) 100,000-fold with 50 mM NaCl, with 2 mL of this suspension added to 8 mL of 50 mM NaCl. Immediately after the particle filtration, the oven was turned on and the temperature set to 110°C for 1 hour to melt the microspheres and fix them to the membrane. The membrane was then flushed with 20 mL of DI water and the hydraulic permeability re-evaluated. Control membranes were generated using the same procedure but with 10 mL of 50 mM NaCl used in place of the particle suspension.

2.4. Stirred Cell Set-up

Ultrafiltration experiments were performed using a 10 mL stirred cell (membrane area of 4.1 cm^2). The stirred cell was placed on a magnetic stir plate (VWR 205 Autostirrer) and connected to an air-pressurized polycarbonate reservoir containing the appropriate feed solution. A stirring speed of 730 rpm was used for all experiments. Pressure was measured using a digital differential pressure gauge (Omega), with permeate (filtrate) collected through the stirred cell outlet.

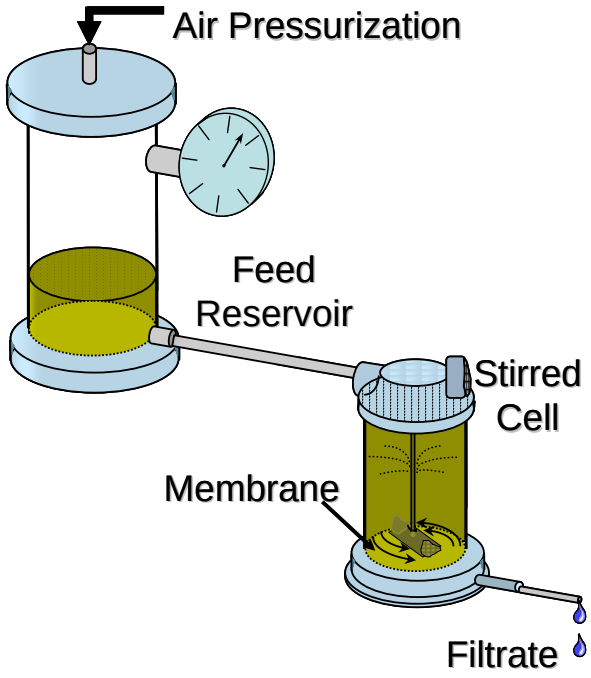

Figure 1: Diagram of Stirred Cell Set-up. Taken from [12]

2.5. Permeability Measurements

The hydraulic permeability was evaluated both before and after pore blockage (to evaluate the effectiveness of the porosity reduction) and also before and after each ultrafiltration experiment (to verify that there was no membrane fouling by the plasmid solution). The filtrate flux was measured by timed volumetric collection at a minimum of three applied pressures. The hydraulic permeability (L_p) was then calculated from the slope of the filtrate flux (J_v) versus pressure (ΔP) data using the following equation:

$$L_p = \frac{J_v}{\Delta P} \qquad (2)$$

2.6. Ultrafiltration Experiments

A fresh plasmid solution was used for each ultrafiltration experiment. The stirred cell and feed tank were filled with the desired plasmid solution, and a small sample was taken directly from the solution in the stirred cell. The system was then pressurized and allowed to stabilize (typically for 2 min of filtration), at which point 1 mL of permeate was collected and discarded to wash out the volume downstream of the membrane. Two successive permeate samples, each of approximately 0.6 mL, were then collected for subsequent analysis of the plasmid concentration. The device was depressurized and a small sample was again taken directly from the stirred cell. This procedure was repeated for multiple applied pressures to evaluate the effect of the filtrate flux on plasmid transmission. All samples were stored at 4°C until analysis.

The observed sieving coefficient was determined as the ratio of the concentration of plasmid in the permeate to the concentration in the feed.

$$S_o = \frac{C_{permeate}}{C_{feed}} \quad (3)$$

The concentration of plasmid in the feed solution was calculated as the arithmetic average of the concentration in the feed samples taken before and after collection of the permeate samples.

2.7. Sample analysis

The plasmid concentration was determined by fluorescence using a GENios FL microplate reader (TECAN). Wells of a 96-well plate (Black Cliniplate, Thermo Fisher Scientific) were filled with 100 µL of the collected feed and permeate samples and with a series of standards containing known concentrations of the desired plasmid. Quant-iT Picogreen dsDNA reagent (Invitrogen) stock solution was diluted 200:1 in TE buffer (Invitrogen), with 100 µL then added to each sample well. The plate was shaken for 3 minutes at 36°C, with the absorbance measured at 535 nm using an excitation wavelength of 485 nm. The plasmid concentration was determined by comparison of the absorbance values with that of the calibration standards.

2.8. Gel Electrophoresis

Agarose gel electrophoresis was used to verify the morphology of the plasmid and also to confirm that there was no plasmid degradation during the ultrafiltration experiments. Gels were made from a 1% agarose solution by dissolving 0.9 g of agarose (EMD Chemicals) in 90 mL of Tris-acetate-EDTA (TAE) buffer (Mediatech, Inc.). The resulting agarose solution was placed in a 55°C water bath. 45 mL of the heated solution was poured into a 7x10 cm gel form and allowed to set. Approximately 15 µL of a given sample was added to each lane along with 3 µL

of TrackIt buffer (Invitrogen). A 6 μL sample of TrackIt 1 kbp DNA ladder (Invitrogen) was used as a reference. The gel was placed in a Mini-Sub Cell GT (Biorad) and run at 55 V for 3 hr in TAE buffer. The gel was then stained with SyBr Gold solution for 24 hours, with images captured using AlphaImager software (Alpha Innotech Corp.).

2.9. SEM imaging

Scanning electron microscopy was used to examine the topography / microstructure of the membrane surfaces. A square sample of membrane (approximately 25 mm^2) was cut from the larger disc and attached to an aluminum barrel stub using carbon tape. A small dab of silver paint was applied to a corner of the sample and the barrel stub, and the paint was allowed to cure overnight. The samples were then sputter-coated with iridium (Ir) to prevent the accumulation of static electron charge during irradiation. The thickness of the Ir coating was approximately 1 to 2 nm. The membrane surfaces were imaged using a JEOL 6700F Field Emission Scanning Electron Microscope (FE-SEM) at magnifications up to 150,000x using a 3.0 to 5.0 kV electron beam.

3. Results and Discussion

3.1. Scanning Electron Microscope (SEM) Analysis of Pores

Sample images of the 15, 30, and 50 nm pore size Nuclepore membranes are shown in Figure 2 at a magnification of 100,000x (Figure 1d shows the 50 nm pore size membrane at a lower magnification). The larger size pores are easily visible as the dark spots surrounded by a white halo. The 50 nm pore size is consistent with measurements taken from the images. The 15 nm pores are very difficult to see in the images, although these were somewhat more readily visible in the original SEM micrographs. There were no overlapping pores ("doublets") in any of the images for the 15 and 30 nm pore sizes, which is consistent with the very low porosity of these membranes [13]. However, a small number of doublets and triplets were observed with the 50 nm pore size membranes due to the close proximity of some of the initial damage tracks. The total number of doublets plus triplets was less than 3% of the number of singlet pores for all samples.

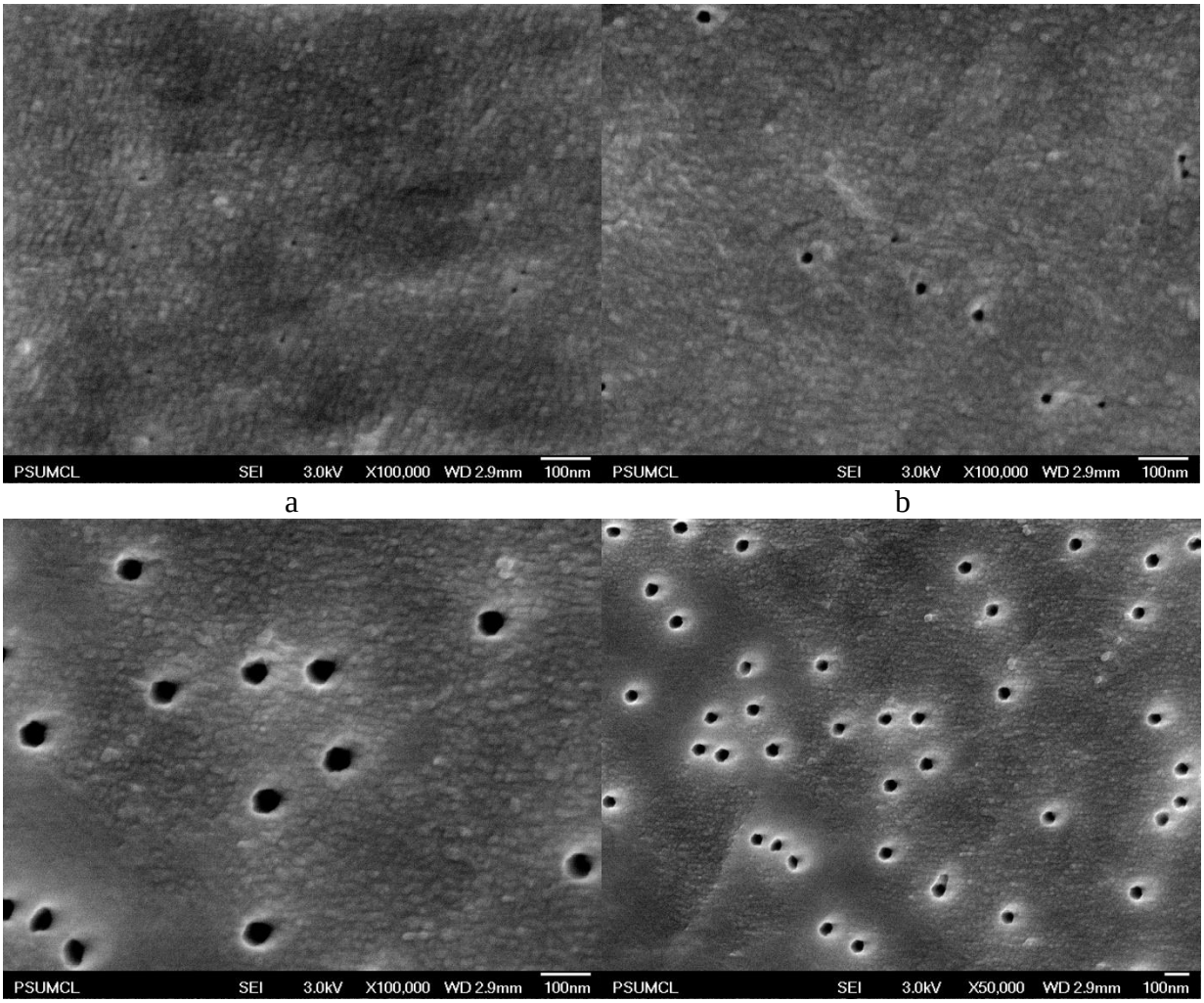

Figure 2: SEM images of Nuclepore Membranes: a) 15 nm pores at 100,000x, b) 30 nm pores at 100,000x, c) 50 nm pores at 100,000x, d) 50 nm pores at 50,000x

The number of pores per unit area was determined directly from the SEM images. In each case, at least 8 pores were counted, with the membrane area determined from the scale bar on the SEM micrographs. Calculations for the 50 nm pores were performed using images at both 100,000x and 50,000x magnification. The membrane porosity was calculated directly from the pore density using the manufacturer's value for the pore diameter (d_p) as:

$$\varepsilon = \frac{N\pi d_p^2}{4} \quad (4)$$

The results are summarized in Table 1 along with the manufacturer's information – the pore density for all of the membranes was reported by the manufacturer as $6x10^8$ pores/cm^2. The measured pore density was considerably larger than that given by the manufacturer based on the SEM images obtained at 100,000x magnification. In contrast, the pore density of the 50 nm membrane calculated from the image obtained at 50,000x magnification was very close to that reported by the manufacturer. This may simply reflect the greater accuracy of the calculations using the 50,000x images, with the calculations performed by averaging results from approximately 30 images each containing at least 20 pores per image. The porosity increased with increasing membrane pore size, but was less than 2.5% for all membranes.

The porosity of the membranes was also calculated from the measured values of the hydraulic permeability (L_p) using the Hagen-Poiseuille equation [10]:

$$\varepsilon = \frac{8\mu\delta_m L_p}{r_p^2} \quad (5)$$

where μ is the viscosity of water, δ_m is the membrane thickness, and r_p is the pore radius. The thickness of all membranes is 6 μm. The porosity calculated from the hydraulic permeability is significantly larger than the values calculated from the SEM images as well as those provided by the manufacturer. Kim and Stevens [14] found similar discrepancies in their analysis of Nuclepore track-etched membranes which they attributed to the flexibility of the polycarbonate films in response to the applied pressure.

Table 1: Pore Density and Porosity of the Nuclepore Membranes

	Manufacturer Information		Calculated from SEM (100,000x)		Hagan-Poiseuille Equation	
d_p (nm)	Pore Density (pores/cm^2)	Porosity	Pore Density (pores/cm^2)	Porosity	Pore Density (pores/cm^2)	Porosity
15	6.E+08	0.11%	7.51E+08	0.13%	9.35E+09	1.65%
30	6.E+08	0.42%	8.45E+08	0.60%	1.56E+09	1.10%
50	6.E+08	1.18%	1.03E+09	2.03%	5.05E+09	9.91%
			6.34E+08*	1.24%*		

*calculated from SEM images at 50,000x

3.2. Gel Electrophoresis

Gel electrophoresis was used to confirm that the plasmid samples were all of the linear isoform and to verify that the plasmid was undamaged during the ultrafiltration experiments. Figure 3 shows a typical agarose gel. The first and last lanes (1 and 8) contain the TrackIt 1 kbp DNA ladder (Invitrogen). Lanes 2 and 4 contain samples of the 3 kbp plasmid feed solution in 10 mM NaCl TE buffer, while lanes 5 and 7 are the feed solution with 150 mM NaCl TE buffer. The plasmids migrate to a position just slightly below that of the 3 kbp linear sample in the DNA ladder; this small difference may simply reflect the different base pair sequence of the pBluescript® plasmid and the linear DNA in the TrackIt DNA ladder. Lane 3 contains a permeate sample obtained during ultrafiltration through the 15 nm Nuclepore membrane at a filtrate flux of 6 µm/s. The band is barely visible, reflecting the high degree of plasmid retention under these conditions. Lane 6 contains a permeate sample from an analogous experiment performed using the higher ionic strength buffer. This band has a much higher intensity,

corresponding to a greater degree of plasmid transmission. This is discussed in more detail subsequently. All samples migrated the same distance through the gel, confirming that there was no damage to the plasmid in any of the ultrafiltration experiments.

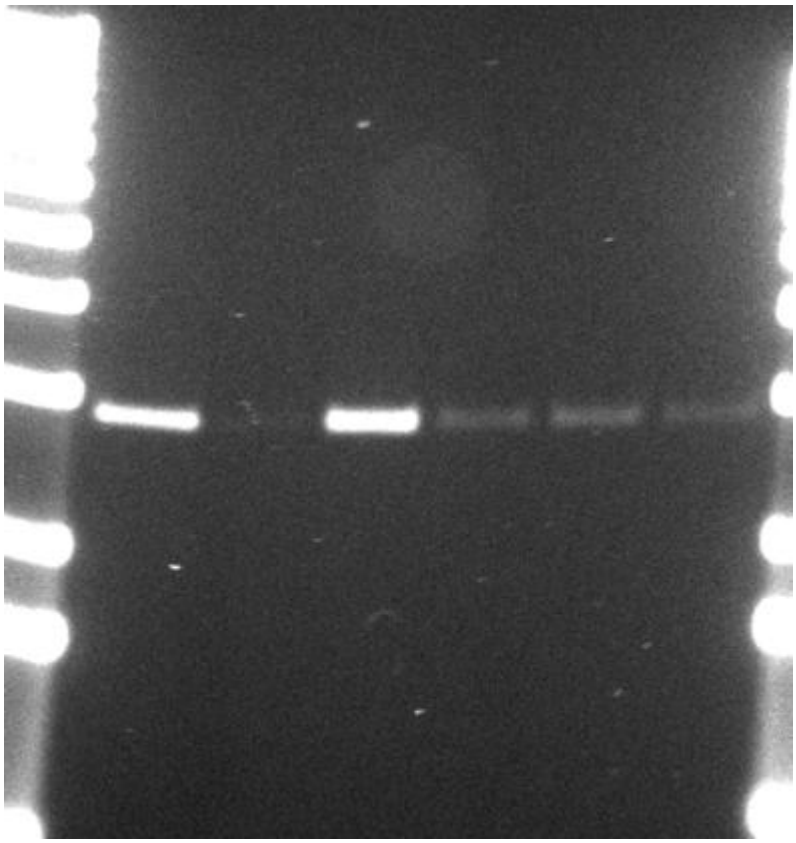

Figure 3: Agarose gel of the 3 kpb linear plasmid. Lanes 1 and 8 contain the DNA ladder. Lanes 2 and 4 contain feed samples from an ultrafiltration experiment with 10 mM NaCl TE buffer while Lanes 5 and 7 contain feed samples with 150 mM TE buffer. Lanes 3 and 6 are permeate samples obtained for experiments with 10 and 150 mM NaCl TE buffer, respectively.

3.3. Effect of Pore Size

Typical experimental data for the observed sieving coefficients of the 3 kbp linear plasmid in 150 mM NaCl TE buffer through the 3 different pore size Nuclepore membranes are shown in Figure 4. The required applied pressure range was greater for the smaller pore size membranes: the data in Figure 4 correspond to pressures of 0.1-2.5 psi for the 50 nm pore size

membrane, 3-16 psi for the 30 nm pore size, and 10-52 psi for the 15 nm pore size. At very low filtrate flux (below 1.5 μm/s), plasmid transmission was negligible for all 3 membranes with S_o < 0.06. The degree of plasmid transmission increased with increasing filtrate flux, with S_o becoming greater than 0.85 for filtrate flux above 5 μm/s for all 3 membranes. At intermediate filtrate flux, the plasmid sieving coefficient increased with increasing pore size. For example, at a filtrate flux of about 2.8 μm/s, the sieving coefficient increased from 0.09 to 0.26 as the pore size increased from 15 to 50 nm.

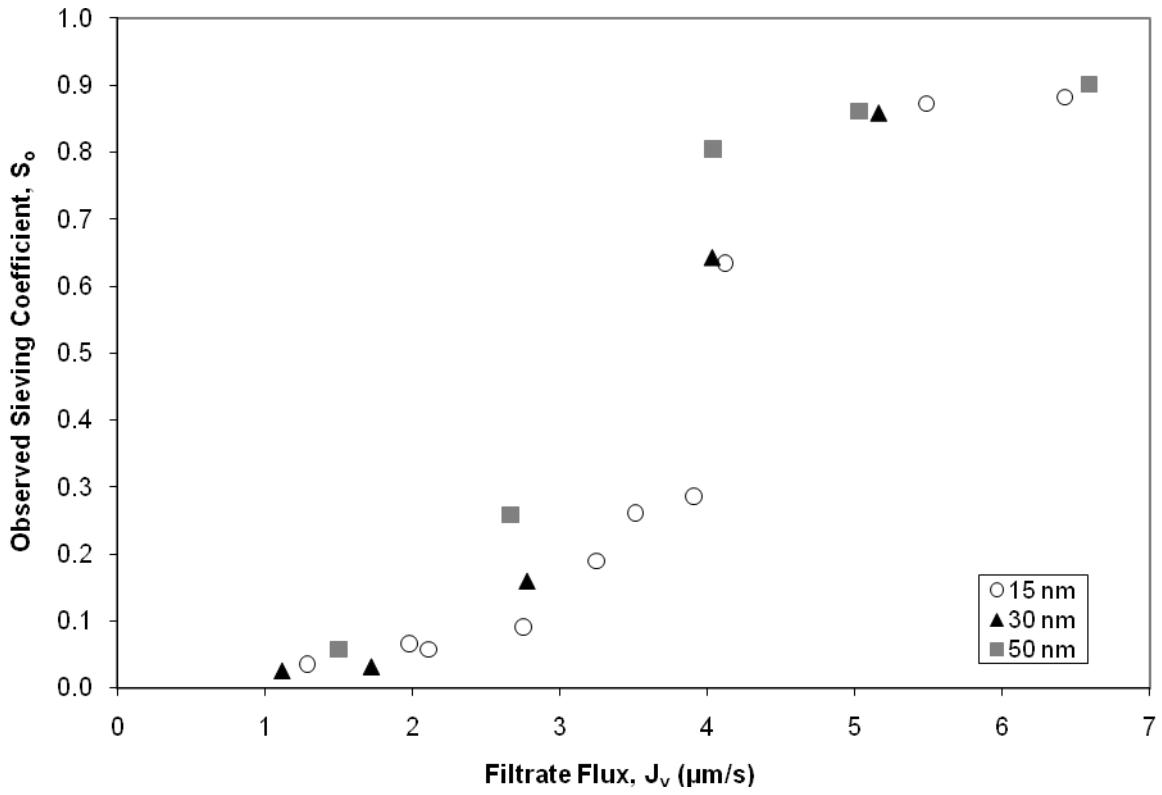

Figure 4: Plasmid sieving coefficient for the different pore size Nuclepore membranes using a 150 mM NaCl TE buffer

The increase in plasmid sieving coefficient with increasing membrane pore size is consistent with the elongation flow model developed by Daoudi and Brochard [15] and subsequently applied to plasmid ultrafiltration by Latulippe et al. using Equation (1):

$$J_{crit} = \left(\frac{\pi^2 D}{R_G^2}\right)\left(\frac{\varepsilon R_S^3}{r_p^2}\right) \quad (1)$$

The pore size dependence predicted by Equation (1) was examined in more detail by plotting the critical flux as a function of the membrane pore diameter. In each case, the critical flux was determined from the observed sieving coefficient data by extrapolating the linear regression fit, determined for S_o values between 0.02 and 0.5, to zero sieving coefficient. The results are shown in Figure 5. The critical flux decreased with increasing pore size as expected. The slope of the data on the log-log plot was n = -0.35, compared to the -2 power predicted by Equation (1). However, this analysis neglects the effect of membrane porosity on the critical flux. According to Equation (4), the porosity scales with r_p^2, thus membranes with the same pore density should have exactly the same critical flux independent of the pore size. This behavior is consistent with the very weak dependence on r_p seen in Figure 5.

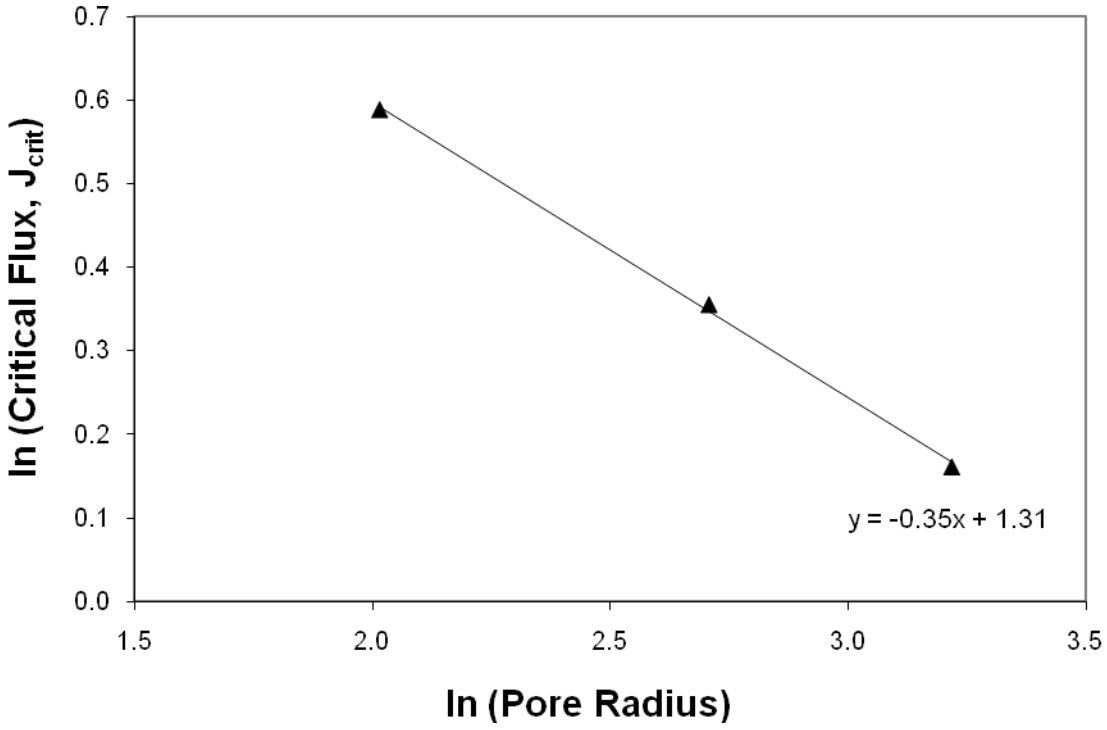

Figure 5: Log-log plot of critical flux as a function of the pore radius for ultrafiltration experiments with the different pore size Nuclepore membranes using 150 mM NaCl TE buffer

3.4. Pore Blocking

Equation (1) predicts a linear dependence of the critical flux on the membrane porosity for membranes with the same pore size. This phenomenon was examined experimentally by performing ultrafiltration experiments through a series of 50 nm pore size membranes in which a fraction of the pores had first been blocked using the polymer particles using the method discussed in section 2. The effectiveness of the pore blocking was evaluated from the change in membrane permeability, since Equation 5 shows that there is a direct relationship between permeability and porosity.

The pores of the 50 nm Nuclepore membrane were blocked with 67 nm polystyrene microspheres. This was initially accomplished by simply filtering a suspension of microspheres through the membrane at high pressure. Although this caused a significant reduction in the membrane permeability, the permeability increased during subsequent plasmid ultrafiltration experiments due to the slow removal (or re-suspension) of the polystyrene microspheres due to stirring of the solution in the ultrafiltration cell.

In order to overcome this problem, the microspheres were "fixed" to the membrane surface by "melting". The glass transition temperature of polystyrene is between 95-107°C [16] while that of polycarbonate is above 150 ^{o}C. The melting was thus performed using an oven temperature of 110°C. Data obtained with a control membrane, which was used to filter a particle-free buffer followed by incubation in the oven, showed a 10-20% decrease in permeability, with the permeability decreasing slightly with increasing incubation time in the oven. The reason for this small reduction in permeability is unknown; it might be due to some deformation of the polycarbonate or it could be due to deposition of NaCl on and within the membrane pores from evaporation of water in the oven.

The membrane that was blocked with microspheres and heated for 60 min showed a 72% reduction in permeability (Table 2). The permeability of this membrane was stable, with the flux varying linearly with pressure (Figure 6) and with no measurable change in permeability after several plasmid ultrafiltration experiments. The use of a 10 min incubation in the oven gave a membrane whose permeability was very similar to that of the control membrane (15% reduction compared to the initial membrane). This may have been due to incomplete melting of the microspheres, allowing the particles to be removed from the membrane when used in the stirred cell. It should also be noted that the membrane that was baked in the oven for only 10 min was

blocked by filtering a suspension of microspheres in deionized water while the membrane that was heated in the oven for 60 min was blocked with microspheres suspended in a salt solution containing 50 mM NaCl. It is thus possible that the different results are due in part to the effect of solution ionic strength on the filtration of the polystyrene microspheres.

Table 2: Percent reduction in membrane hydraulic permeability for a control membrane and for a membrane blocked with polystyrene microspheres after heating at 110°C

	60 min	20 min	10 min
Control	17-20%	15%	11%
Blocked	72%	--	15%

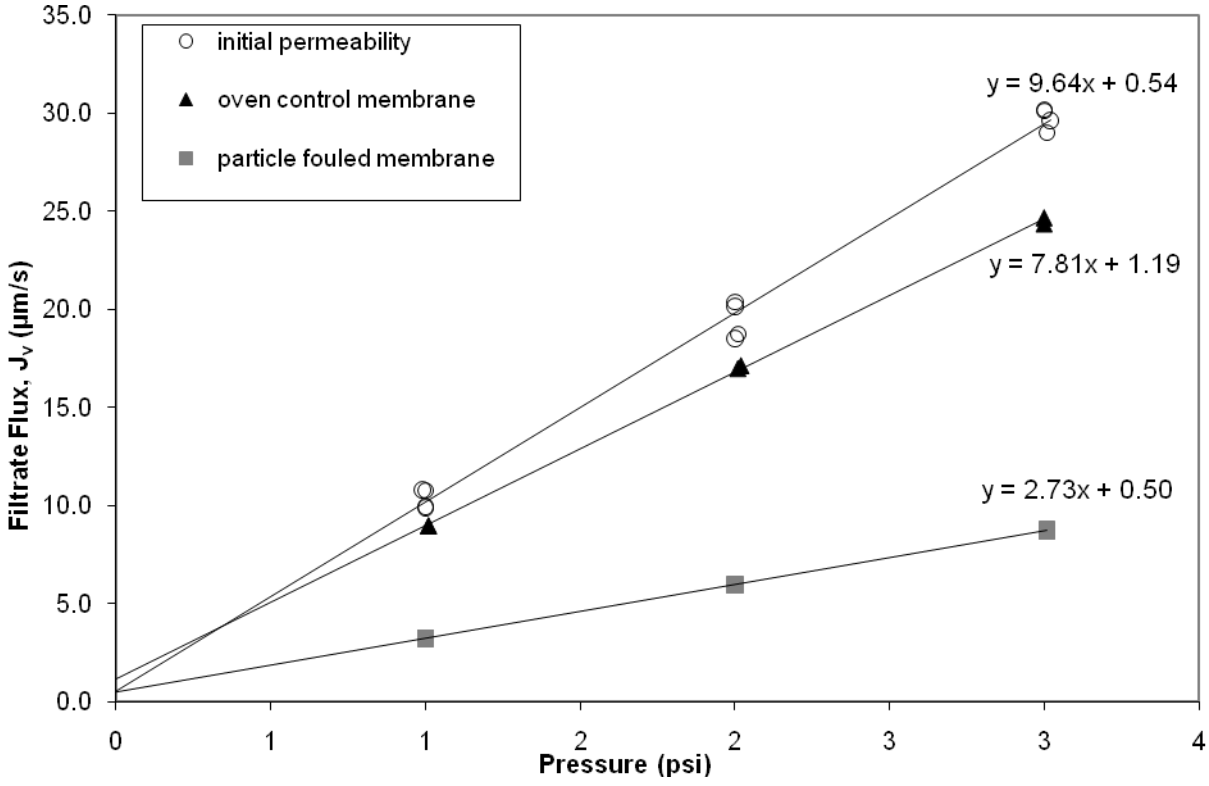

Figure 6: Permeabilities of control and particle blocked membranes after incubation at 110°C for 1 hour

Figure 7 shows an SEM image of a control membrane (heated for 60 min at 110 ^{o}C but without any particles) and a membrane that was "blocked" using the 67 nm polystyrene microspheres. The microspheres are easily visible on the surface of the membrane, with many of these spheres clearly melted into the pores. There also appear to be spheres simply sitting on the upper surface of the membrane. The calculated pore density for the blocked membrane was 73% less than that of an untreated membrane, in excellent agreement with the measured change in the membrane permeability. Some of the pores in the control membrane do appear to be at least partially blocked, although the origin of this effect is unknown. The calculated pore density for the control membrane was 36% smaller than that of an unmodified membrane, which is even greater than the reduction permeability seen in Table 2. The SEM images clearly demonstrate that the pore blockage technique used in this thesis is effective at reducing the membrane porosity, although there may well be artifacts associated with a change in pore structure simply due to the 60 min heating in the oven.

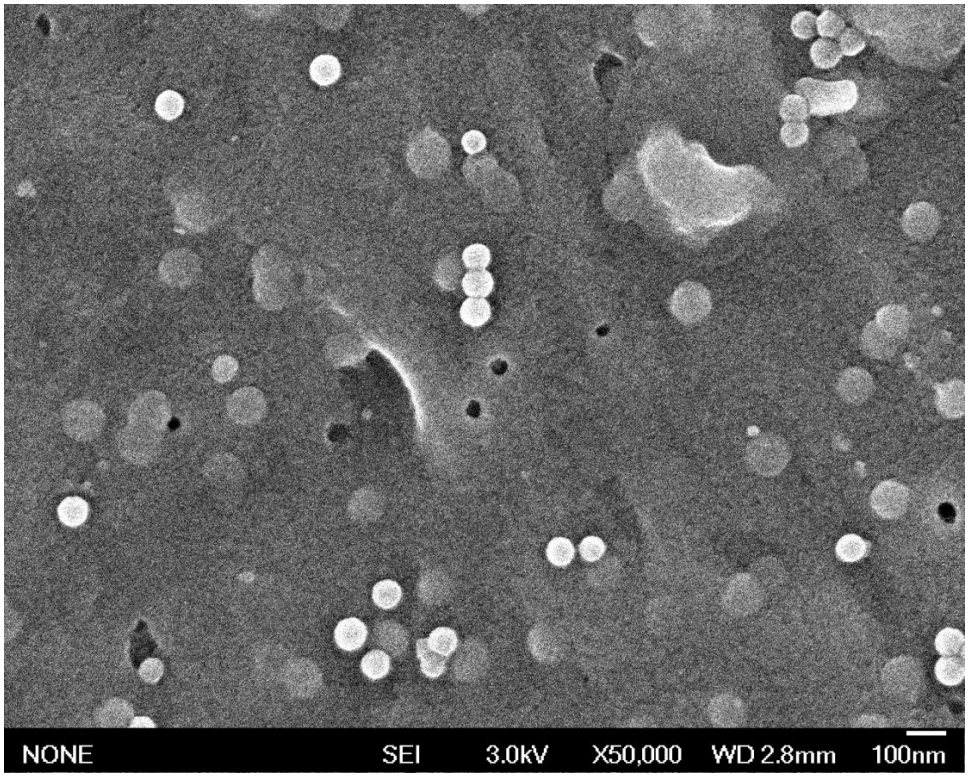

a) 50 nm Nuclepore membrane blocked with 67 nm polystyrene particles

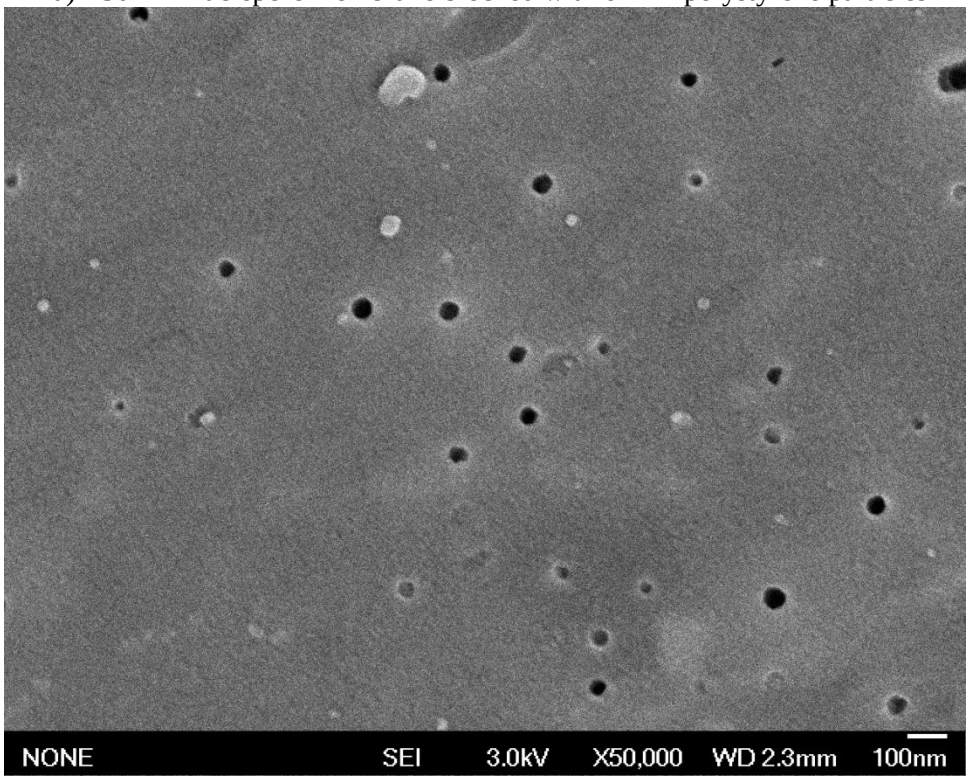

b) 50 nm Nuclepore control membrane (heated in the oven)

Figure 7: Blocked and control membranes after oven processing and ultrafiltration experiments

3.5. Effect of Porosity

Figure 8 shows the effects of membrane porosity on the plasmid sieving coefficients. The sieving coefficients for the unmodified and control (heated but with no microspheres) membranes were nearly identical over the entire range of filtrate flux, consistent with the relatively small difference in permeability (and thus porosity) for these membranes. In contrast, the sieving coefficients for the membrane with low porosity (blocked with microspheres) are significantly greater than those for the unmodified membrane. For example, at a filtrate flux of about 3.5 μm/s, the plasmid sieving coefficient for the native Nuclepore membrane was only 0.13 while that for the low porosity membrane was 0.87, a difference of more than 6-fold.

The critical flux was determined by extrapolating the sieving coefficient data to S_o=0 as discussed previously, giving J_{crit} = 1.3 μm/s for the low porosity membrane and 2.9 μm/s for the unmodified membrane. This increase in critical flux is in good agreement with the linear dependence on porosity given by Equation (1). The ratio of the permeability of the unmodified membrane to that of the low porosity membrane was 2.5, which should also be equal to the ratio of the porosities since the membrane thickness and pore density were unaffected by the pore blockage procedure, while the ratio of the critical flux value was 2.2.

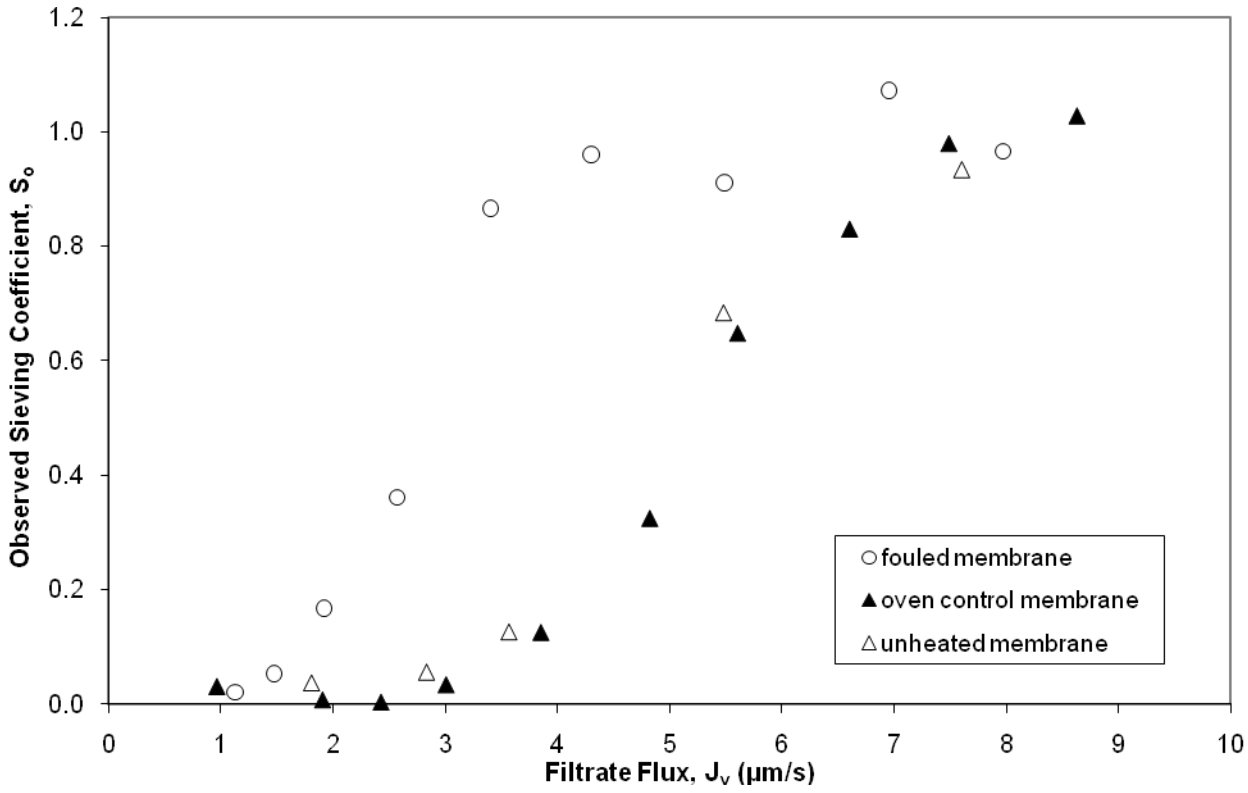

Figure 8: Plasmid sieving coefficient for the unmodified, the control, and the low porosity membrane using 10 mM NaCl TE buffer

3.6. Effect of Solution Ionic Strength

Ultrafiltration experiments were also performed at two different ionic strengths: TE buffer with added 10 mM NaCl and with added 150 mM NaCl. Results are shown in Figure 9 using the 15 nm and 50 nm pore size membranes. In both cases, the sieving coefficients increase with increasing ionic strength. The dependence on ionic strength is much greater with the smaller pore size membrane. For example, at a filtrate flux of 5-6 µm/s, the sieving coefficient increases from 0.7 to 0.9 with increasing NaCl concentration for the 50 nm pore size membrane

compared to a 9-fold increase for the 15 nm pore size membrane. Similar behavior was seen with the calculated values of the critical filtrate flux. The critical flux for the 15 nm pore size membrane was 1.8 μm/s in the 150 mM NaCl. The critical flux could not be determined with the 10 mM NaCl because significant plasmid transmission was not seen at any of the filtrate fluxes studied, although the data clearly indicate that $J_{crit} > 6$ μm/s under these conditions. The increase in critical flux for the 50 nm pore size membrane was over 200% (from $J_{crit} = 2.8$ μm/s to 1.2 μm/s) as the salt concentration increased from 10 to 150 mM NaCl. (Due to the absence of data for S_o between 0.3 and 0.6, the critical flux was calculated with using data up to $S_o = 0.7$).

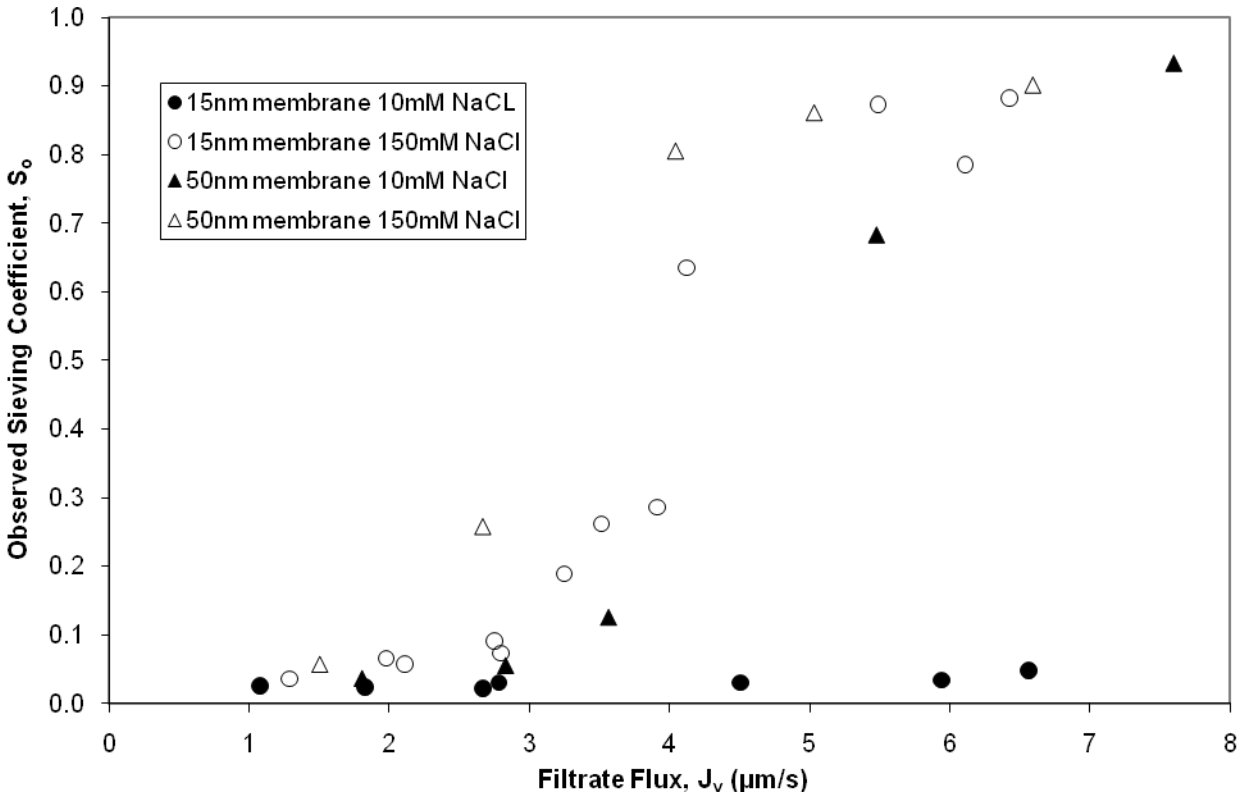

Figure 9: Effect of solution ionic strength on plasmid sieving coefficients for the 15 nm and 50 nm pore size Nuclepore membranes

An analogous set of ultrafiltration experiments were performed with the control and low porosity membranes (Figure 10). The plasmid transmission was again greater at the higher salt concentration. The critical flux for the low porosity membrane increased from 1.1 to 1.3 μm/s as the NaCl concentration was decreased from 150 to 10 mM, with a similar variation seen with the control membrane.

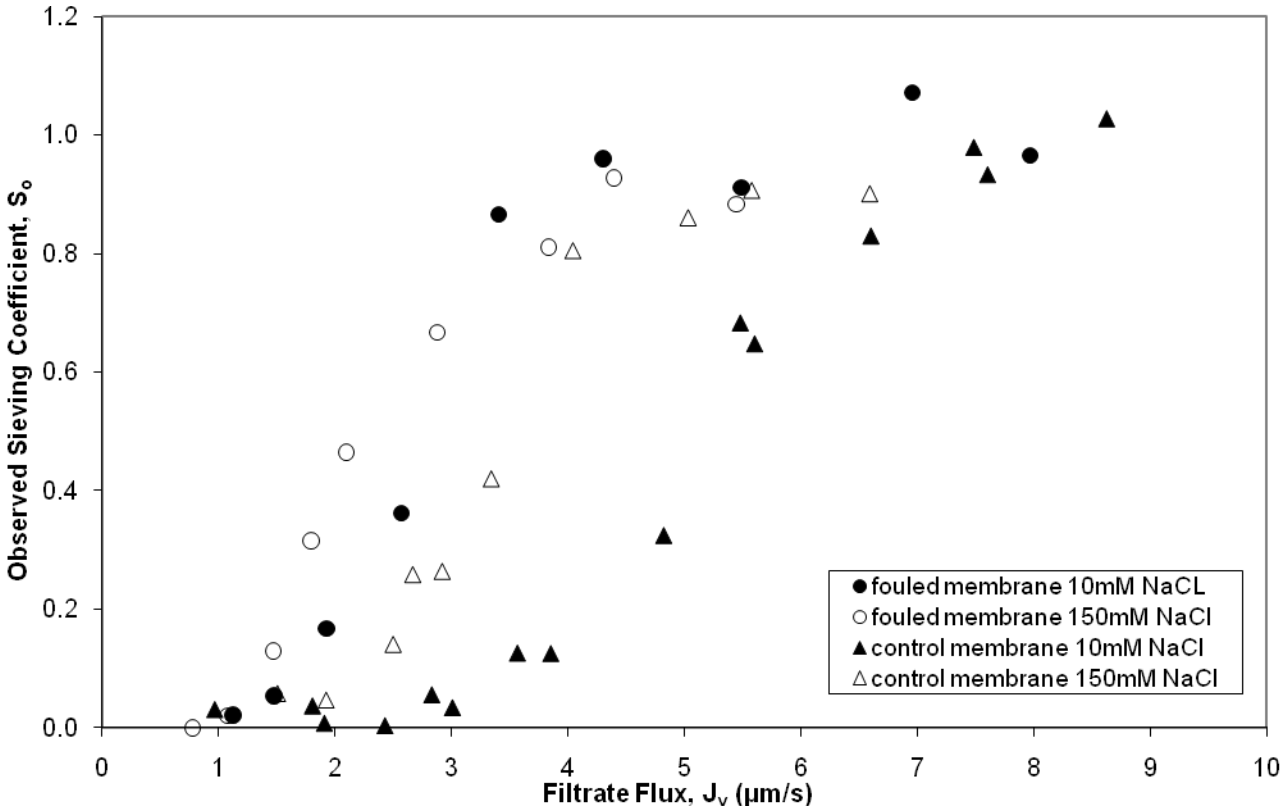

Figure 10: Effect of solution ionic strength on plasmid sieving coefficients for the control and low porosity versions of the 50 nm pore size Nuclepore membranes

3.7. Membrane Comparison

Figure 11 shows a comparison of the observed sieving coefficient data for the 15 nm pore size Nuclepore membrane with that of a 300 kD Ultracel composite regenerated cellulose membrane. The data for the Ultracel membrane appear shifted to the right compared to the results for the Nuclepore membrane, with the magnitude of this shift being around 2 – 6 μm/s. At any given filtrate flux, the plasmid sieving coefficient through the Nuclepore membrane was significantly greater than that through the Ultracel membrane, even though these membranes have similar pore size (Latulippe et al. [6] estimated the pore diameter of the 300 kD Ultracel membrane as approximately 19 nm). For example, at a filtrate flux of approximately 4.3 μm/s, the sieving coefficient through the Nuclepore membrane was greater than 0.6 while that through the Ultracel membrane was less than 0.02. A similar difference was seen in the critical flux with values of 1.8 μm/s for the Nuclepore membrane and 3.9 μm/s for the Ultracel. This difference in critical flux is likely due to the difference in porosity of these membranes; the porosity of the Nuclepore membrane is less than 1% while that of the Ultracel 300 kDa has been previously reported as 50%.

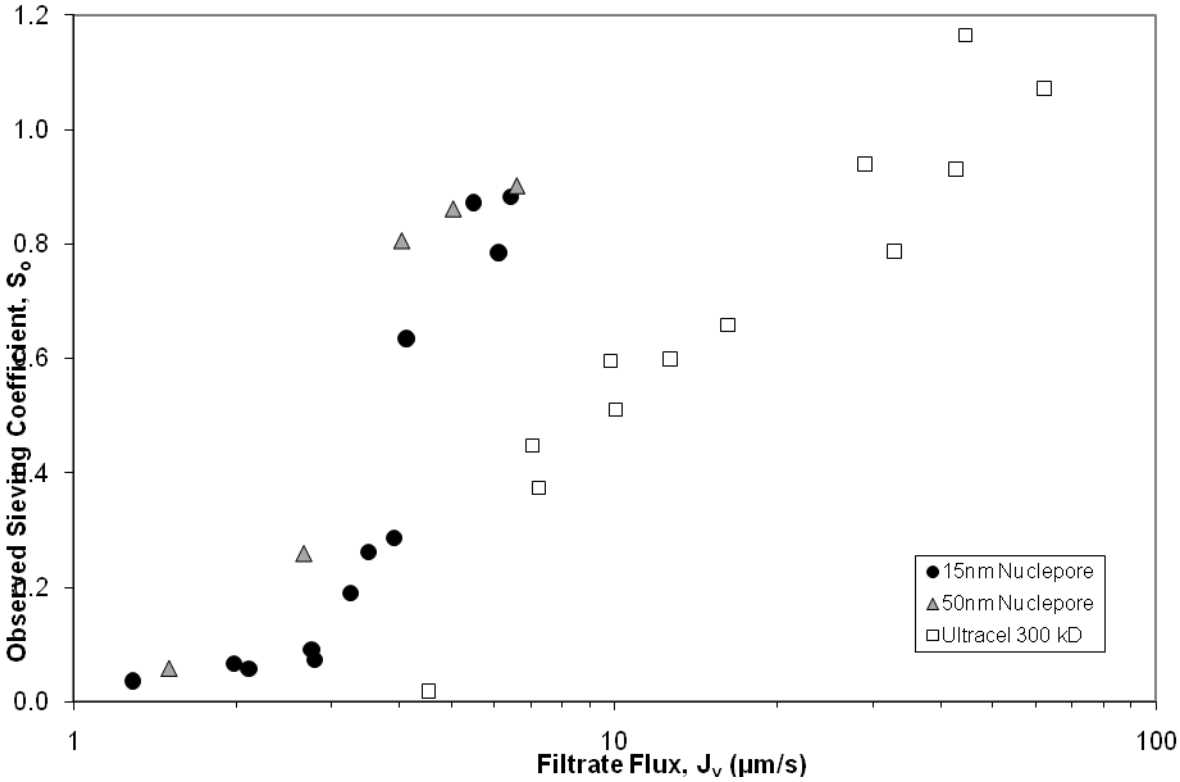

Figure 11: Plasmid sieving coefficient for Nuclepore and Ultracel membranes using a 150 mM NaCl TE buffer (Ultracel data from D.R. Latulippe [12])

4. Conclusions

This thesis provides the first experimental data for the transmission of a 3 kbp plasmid through a series of Nuclepore membranes with very uniform cylindrical pores with diameters of 15 nm, 30 nm, and 50 nm. The plasmid sieving coefficient was essentially zero at low values of the filtrate flux, increasing to more than 80% transmission at high filtrate flux. This general behavior is consistent with previous results obtained with Ultracel composite regenerated cellulose membranes and with predictions of the elongational flow model developed by Daoudi and Brochard [15] and subsequently extended by Latulippe et al. [6]. The critical flux obtained with the 15 nm pore size Nuclepore membrane was about 2-fold smaller than that found with the 300 kD Ultracel membrane even though these membranes have dramatically different porosities (less than 1% for the Nuclepore and as high as 50% for the Ultracel 300 kDa). One possible explanation for this discrepancy is that the surface porosity of the Ultrcel membrane may be much smaller than the bulk porosity. For example, Yoon et al. [17] reported that the surface porosity of an Amicon XM300 membrane (which also has a 300 kDa nominal molecular weight cut-off) is less than 4%, which would bring these results into much better agreement with the predictions of the elongational flow model.

In order to examine the effects of membrane porosity on plasmid transmission in more detail, experiments were performed with Nuclepore membranes having reduced porosity. These low porosity membranes were formed by blocking some of the pores using polystyrene microspheres, with.the pore blockage stabilized by melting the particles in place by heating the membrane in an oven. The plasmid transmission through these low porosity membranes was significantly greater than that of the un-modified membrane (at a given filtrate flux), and the

critical flux values appear to scale linearly with the porosity, both of which are consistent with predictions of the elongational flow model. These results provide the first experimental verification of the predicted dependence of the critical flux on the membrane porosity for membranes with identical pore size and pore morphology.

Another significant difference between the Nuclepore membranes and the cellulose membranes is the highly uniform pore size for the track-etched Nuclepore membranes. Latulippe et al. [6] hypothesized that the gradual increase in plasmid transmission with increasing filtrate flux seen experimentally with the Ultracel membranes might have been due to their broad pore size distribution; the elongational flow model developed by Daoudi and Brochard [15] predicts a sharp transition from zero to 100% transmission at the critical flux. For example, data obtained with the 300 kD Ultracel membrane showed a transition from $S_o \approx 0$ to $S_o \approx 1$ as the filtrate flux increased from 7 to 60 μm/s, nearly a 9-fold range in flux. The data obtained with the Nuclepore membranes show a similar transition, with the plasmid transmission increasing from 0 to nearly 100% as the filtrate flux varies from about 1 to 9 μm/s. These data strongly suggest that the gradual increase in plasmid transmission is unrelated to the presence of a membrane pore size distribution given the very large differences in the breadth of the pore size distribution for the Ultracel and Nuclepore membranes. Instead, this transition may reflect the range of properties / conformations of the plasmid itself or it could be due to limitations in the application of the simple elongational flow model to describe plasmid transmission during ultrafiltration. Additional work will be required to develop a more complete understanding of this behavior and its implications for the use of membrane systems for plasmid purification.

5. References

[1] Kelly, W.J., Perspectives on plasmid-based gene therapy: challenges for the product and the process, *Biotechnology Applied Biochemistry*, 37 (2003) 219-223.

[2] Prather, K.J., Sagar, S., Murphy, J., and M. Chartrain, Industrial scale production of plasmid DNA for vaccine and gene therapy: plasmid design, production, and purification, *Enzyme and Microbial Technology*, 33 (2003) 865-883.

[3] Prazeres, D.M.F, and G.N.M. Ferreira, Design of flowsheets for the recovery and purification of plasmids for gene therapy and DNA vaccination, *Chemical Engineering and Processing*, 43 (2004) 615-630.

[4] Pereira, L.R., Prazeres, D.M., and M. Mateus, Hydrophobic interaction membrane chromatography for plasmid DNA purification: Design and optimization, *Journal of Separation Science*, 33 (2010) 1-10.

[5] Kong, S., Titchener-Hooker, N., and M.S. Levy, Plasmid DNA processing for gene therapy and vaccination: Studies on the membrane sterilization filtration step, *Journal of Membrane Science*, 280 (2006) 824-831.

[6] Latulippe, D.R., Ager, K., and A.L Zydney, Flux-dependent transmission of supercoiled plasmid DNA through ultrafiltration membranes, *Journal of Membrane Science*, 294 (2007) 169-177.

[7] Latulippe, D.R., and A.L. Zydney, Salt-induced changes in plasmid DNA transmission through ultrafiltration membranes, *Biotechnology and Bioengineering*, 99 (2008) 390-398.

[8] Apel, P., Track etching technique in membrane technology, *Radiation Measurements*, 34 (2001) 559-566.

[9] Chun, K.Y., and P. Stroeve, Protein transport in nanoporous membranes modified with self-assembled monolayers of functionalized thiols, *Langmuir*, 18 (2002) 4653-4658.

[10] Deen, W.M., Hindered transport of large molecules in liquid-filled pores, *AIChE Journal*, 33 (1987) 1409-1425.

[11] Ho, C.C., and A.L. Zydney, Effect of membrane morphology on the initial rate of protein fouling during microfiltration, *Journal of Membrane Science*, 155 (1999) 261-275.

[12] Latulippe, D.R., Ph.D. Thesis, Department of Chemical Engineering, The Pennsylvania State University (2010).

[13] Kim, K.J., Stevens, P.V., and A.G. Fane, Porosity dependence of pore entry shape in track-etched membranes by image analysis, *Journal of Membrane Science*, 93 (1994) 79-90.

[14] Kim, K.J., and P.V. Stevens, Hydraulic and surface characteristics of membranes with parallel cylindrical pores, *Journal of Membrane Science*, 123 (1997) 303-314.

[15] Daoudi, S., and F. Brochard, Flows of flexible polymer solutions in pores, *Macromolecules* 11 (1978) 751-758.

[16] Rieger, J., The glass transition temperature of polystyrene, *Journal of Thermal Analysis*, 46 (1996) 965-972.

[17] Yoon, K., Kim, K., Wang, X., Fang, D., Hsiao, B.S., and B. Chu, High flux ultrafiltration membranes based on electrospun nanofibrous PAN scaffolds and chitosan coating, *Polymer*, 47 (2006) 2434–2441.

Academic Vita Allison B. Harter

abh5013@psu.edu
abharter@gmail.com

EDUCATION

B.S. Chemical Engineering with honors (Spring 2010)
The Pennsylvania State University, University Park, PA
Schreyer Honors Scholar

B.S. French and Francophone Studies: French-Engineering Option
Minor in International Studies
Study Abroad in Besançon, France- Summer 2006
Study Abroad in Montpellier, France- Spring 2008

WORK EXPERIENCE

Centocor Research & Development- Spring House, PA **June 2009-December 2009**

- Pharmaceutical Development Systems- Validation Engineering
- Support GMP pilot plant through validation activities
- Assist in process and automation design and equipment specification

Merck & Co., Inc.- Rahway, NJ **May 2008-August 2008**

- Chemical Process Development and Commercialization
- Engineering and Technology Fellowship Award
- Produce analytical data to support Quality by Design

DuPont, Chambers Works- Deep Water, N.J. **May 2007-August 2007**

- Secure Environmental Treatment
- Process safety management documentation for wastewater treatment
- Analyze compliance with government regulations at waste acceptance

The Pennsylvania State University
Honors Thesis and Research- Chemical Engineering **Fall 2008-Spring 2010**

- Separate linear DNA plasmids through ultrafiltration

Women in Science and Engineering Research Program **Spring 2006-Spring 2007**

- Perform laboratory research comparing membranes and separating proteins

Women in Engineering Program Facilitator **Fall 2006-Spring 2009**

- Aid engineers in their study of introductory math courses

LEADERSHIP

Phi Sigma Rho- Women in Engineering Sorority **Fall 2006-Present**

- Treasurer- 2008-2009
- Membership Educator- Fall 2007

Schreyer Honors College Mentor- Fall 2006, Fall 2007
Engineering Mentorship Program- Fall 2006, Fall 2007
Schreyer Honors College Student Council **Fall 2005-Present**

- Member of Academic and Recruitment Committees

Penn State Dance Marathon (THON) **Fall 2005-Present**

- Fundraise for Four Diamonds Fund, benefiting pediatric cancer
- Rules and Regulations Committee Member 2006, 2007
- Dancer 2009

HONORS

- Evan Pugh Junior and Senior Scholar Award **(Spring 2008, Spring 2009)**
- The President's Sparks Award- Penn State University **(Spring 2007)**
- The President's Freshman Award- Penn State University **(Spring 2006)**
- Schreyer Academic Excellence Scholarship **(Fall 2005-Present)**
- College of Engineering Scholarship **(Fall 2005-Present)**

SKILLS

Working knowledge of Microsoft Word, Excel, PowerPoint; Mathematica; MATLAB
Extensive experience with high performance liquid chromatography
Proficient in French (France home stay for 6 months)